Available online at www.sciencedirect.com
ScienceDirect
Trans. Nonferrous Met. Soc. China 23(2013) 1472−1479
Transactions of Nonferrous Metals Society of China
www.tnmsc.cn

Relationship between $Al(OH)_3$ solubility and particle size in synthetic Bayer liquors

Xiao-bin LI, Li YAN, Dong-feng ZHAO, Qiu-sheng ZHOU, Gui-hua LIU, Zhi-hong PENG, Shuai-shuai YANG, Tian-gui QI

School of Metallurgy and Environment, Central South University, Changsha 410083, China

Received 1 August 2012; accepted 4 December 2012

Abstract: Surface tension of sodium aluminate solution and the contact angle between $Al(OH)_3$ particles and aluminate solution were measured, then the dependence of $Al(OH)_3$ solubility on its particle size was calculated and thus the variation of the critical nucleus sizes was determined based on the Ostwald ripening formula. The results show that the $Al(OH)_3$ solubility in sodium aluminate solution decreases with the increment of particle size, and the critical nucleus sizes increase with the rise of alkali concentration, caustic ratio and precipitation temperature. The results also imply that the presence of small particles in seeded precipitation system is an important factor to limit the depth of precipitation.

Key words: Bayer liquor; $Al(OH)_3$; interfacial property; solubility; critical nucleus size

1 Introduction

The precipitation of $Al(OH)_3$ from sodium aluminate solution is a key step of Bayer process to the quality of the products and efficiency of the alumina production. However, no breakthrough progress for the seeded precipitation process has been achieved over the past decades; especially the serious contradiction between the increase of precipitate rate and the improvement of product quality has not been well solved [1].

The supersaturated Bayer liquors are quite different from the ordinary inorganic salt solutions and very difficult to nucleate spontaneously. For alumina production, a large number of seeds must be added to reduce the induction period of nucleation so as to promote the precipitation of $Al(OH)_3$ [2]. Generally, the seeded precipitation process of sodium aluminate solution involves the following steps: 1) with the induction effects of seeds, the evolution of other aluminate species to the favorable precipitate units in the aluminate solution [3], 2) formation of Al(III)-containing ion clusters [4] of favorable precipitate unit, and 3) precipitation of $Al(OH)_3$ by secondary nucleation or growth. Therefore, the seeded precipitation of sodium aluminate solution belongs to the solid−liquid binary-phase system containing the Bayer liquors and the charged solid particles. In order to investigate the precipitation mechanism so as to intensify the precipitation process, many studies focus on two aspects: 1) the structure of aluminate anions and the physico-chemical properties of sodium aluminate solution [5−8] and 2) the behavior of $Al(OH)_3$ particles [9,10].

The $Al(OH)_3$ precipitation process of aluminate solution heavily depends on the interfacial properties between the solid and the solution. In terms of thermodynamics and kinetics, the precipitate efficiency to some extent relies on the equilibrium concentration of $Al(OH)_3$ particles in the late period; moreover, the solubility is determined by the smallest particles in the crystal population distribution system. Additionally, the particle size greatly affects the ratio of agglomeration and growth and thus affects the particle size distribution of products. Although the industrial precipitation process with a great number of seeds is quite different from the homogeneous process and its physicochemical processes are more complicated, the common feature is that the favorable precipitate units transfer from liquid phase to solid phase. Therefore, the investigation of the size of the

Foundation item: Project (51274242) supported by the National Natural Science Foundation of China
Corresponding author: Dong-feng ZHAO; Tel: +86-731-88877830; E-mail: qitiangui@csu.edu.cn
DOI: 10.1016/S1003-6326(13)62619-9

smallest particle being compatible with aluminate solution, i.e. the critical nucleus size, is a very important research project. Ordinarily, the critical nucleus size is determined through measuring the induction period of the spontaneous precipitation and then calculating based on the homogeneous nucleation theory. For example, ROSSITER et al [11] measured the induction period of homogeneous nucleation in terms of the changes of liquor turbidity by a multi-angle laser scanning equipment, then obtained a interfacial tension of (45±6) mJ/m^2 and a critical nucleus size of (0.0012±0.0001) μm at 333 K by using the nucleation rate equation and the Ostwald ripening formula, respectively. ZHANG et al [12] measured the induction period of aluminate solution with different supersaturations with an in-situ conductivity analyzer, and then determined the interfacial energy of 34−35 mJ/m^2 and the critical nucleus size of 1.5−2.0 μm by the same method employed by ROSSITER et al. But LI et al [13] reported the interfacial tensions of approximate 106 mJ/m^2 and the critical nucleus size of 1.1−1.8 μm by the Gibbs-Kelvin formula at 323 K and 333 K.

The differences of the solid−liquid interfacial tension and the critical nucleus size reported above may be attributed to 1) the discrepancy of the measured induction period due to the fact that any method for determining the induction period cannot accurately separate nucleation and growth, and the measured induction period includes the nucleation time and growth time (from nucleus to the detectable size); 2) without considering the activity coefficient due to the fact that generally, it is feasible for coarse particle to substitute the concentration for the activity as its solubility is close to the equilibrium concentration, but for the fine particle, the difference of activity coefficient cannot be neglected as its solubility is much larger than the equilibrium concentration; 3) neglecting the variation of solid−liquid interfacial energy. Theoretically, the solid−liquid interfacial energy is affected by both the particle size and the liquid properties. The above mentioned studies are limited to some special conditions, which are not enough for the precipitation system with a great change in composition and temperature.

Under those considerations, this work presents a study of the relationship between $Al(OH)_3$ solubility and particle size in synthetic Bayer liquors based on the solid−liquid interfacial properties under different conditions, attempting to provide a guidance for adjusting the behavior of $Al(OH)_3$ particles in seeded precipitation process.

2 Experimental

2.1 Liquor preparation and analysis

AR grade sodium hydroxide pellets and $Al(OH)_3$ powder (Tianjin Kermel Chemical Reagent Ltd., China) were dissolved in deionized water under the heating and stirring condition. And then the obtained solution was filtered twice to get the synthetic Bayer liquor for experiments. The concentration of sodium hydroxide as Na_2O and the concentration of aluminum species as Al_2O_3 were determined by titration using a variation of the Watts-Utley method [14]. The caustic ratio of liquors (α_k) was defined as the molar ratio of Na_2O to Al_2O_3.

2.2 Experimental procedure

The required amount of sodium aluminate solution was poured into a 2 L stainless steel precipitation vessels immersed in a thermostat water bath with temperature-controlled precision of ±1 °C. As the solution was preheated to the preset temperature, weighed industrial $Al(OH)_3$ seed (from CHALCO, $w(Al_2O_3)$>64.5%, $w(SiO_2)$<0.02%, $w(Fe_2O_3)$<0.02%) was added to the precipitation vessels and agitation was started with 140 r/min. The composition of spent aluminate solution was determined by titration and the precipitation ratio (η) was calculated by $\eta=(1-\alpha_{k0}/\alpha_{k,t})\times100\%$, where α_{k0} and $\alpha_{k,t}$ denote caustic ratios of liquors at the initial stage and at time t, respectively.

2.3 Analysis instruments and methods

1) Liquid surface tension analysis. The surface tension apparatus (KRUSS-K100, GER) was connected to a water bath with temperature-controlled precision of ±0.5 °C. The sodium aluminate solution was poured into the testing container and then preheated for 30 min to the required temperature. The liquid surface tensions were determined by the Wilhelmy-Plate method.

2) Infrared spectroscopy analysis. The IR spectra of thin films of sodium aluminate solution on KBr plate were collected on a spectrometer with 4 cm^{-1} resolution (FT-IR 6700, Nicolet Co., USA). The whole process was in a nitrogen atmosphere.

3) Contact angle analysis. The $Al(OH)_3$ powders (~5 g) was compressed into a thin plate (pressure ~10 MPa) by a tablet pressing machine (YP-2, Shanghai Shanyue Technology Instrument Ltd., China), then the contact angles of testing liquors on $Al(OH)_3$ plate were determined with a contact angle meter (CL200B, Shanghai Solon Information Technology Ltd., China).

4) SEM analysis. The morphology of the product was observed by scanning electron microscopy (JSM-6360LV, Electronic Ltd., Japan).

3 Results and discussion

3.1 Determination of solid−liquid interfacial tension

The possibility of estimating solid surface tensions from contact angles relies on a relation recognized by

YOUNG in 1805. The contact angle of a liquid drop on a solid surface is defined by the mechanical equilibrium of the drop under the action of three interfacial tensions [15]:

$$\gamma_{sl} = \gamma_{sv} - \gamma_{lv}\cos\theta \quad (1)$$

where γ_{sl} is the solid−liquid interfacial tension; γ_{sv} is the solid surface free energy; γ_{lv} is the liquid surface tension; θ is the contact angle between solid phase and liquid phase.

In order to determine the solid−liquid interfacial tension, the solid surface free energy, the liquid surface tension and the contact angle were measured and calculated.

1) Solid surface free energy

As the particle size distribution of the powder may have an impact on the contact angle, the Bayer industrial $Al(OH)_3$ powder was screened. Figure 1 shows the particle size distribution curves of screened $Al(OH)_3$ powder samples.

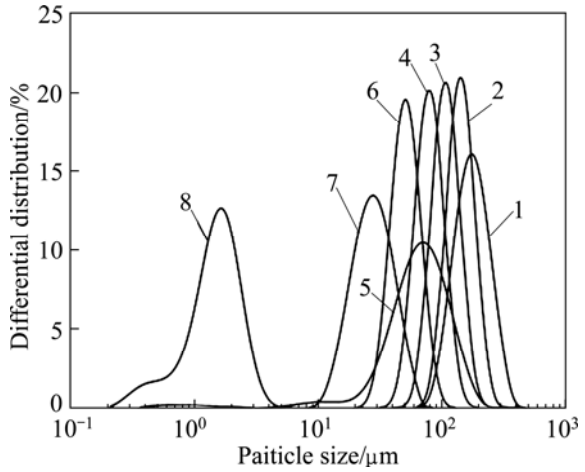

Fig. 1 Particle size distribution curves of screened $Al(OH)_3$ powder samples with different volume average particle diameters: 1—196.04 μm; 2—156.33 μm; 3—118.30 μm; 4—87.44 μm; 5—77.40 μm; 6—56.30 μm; 7—31.47 μm; 8—1.67 μm

The contact angles of the liquids glycerol-diiodomethane on the $Al(OH)_3$ plates prepared from different samples were measured, and then the solid surface free energy was calculated according to Eqs. (2) and (3), as shown in Table 1.

OWENS and WENT [16] developed a two-parameter system to describe the inter forces between the molecules and an estimation method of surface free energy, which was mainly applied to the special solid surface and testing liquid:

$$\gamma_{lv}(1+\cos\theta) = 2(\gamma_s^D\gamma_l^D)^{1/2} + 2(\gamma_s^P\gamma_l^P)^{1/2} \quad (2)$$

$$\gamma_{sv} = \gamma_s^D + \gamma_s^P \quad (3)$$

where γ_l^D is the liquid dispersion force; γ_l^P is the liquid polar force; γ_s^D is the solid dispersion force; γ_s^P is the solid polar force.

Table 1 Surface free energy of industrial $Al(OH)_3$ powder samples

No.	D[4,3]/ μm	θ_1(glycerol)/ (°)	θ_2(diiodomethane)/ (°)	γ_{sl}/ (mJ·m^{-2})
1	196.04	60.63	18.15	48.58
2	156.33	66.87	21.24	48.92
3	118.30	52.28	20.95	47.89
4	87.44	48.70	20.35	48.70
5	77.40	51.11	21.90	47.84
6	56.30	57.37	16.07	48.86
7	31.47	58.58	19.46	47.98
8	1.67	48.73	26.85	48.59

D[4,3] denotes the volume average particle diameter; Sample 5 is industrial $Al(OH)_3$ powder.

Table 1 indicates that the values of surface free energy of industrial $Al(OH)_3$ powders with different particle size distribution (D[4,3]=1.67−196.04 μm) are about 48 mJ/m^2 with the variation of 1 mJ/m^2, which means that there is no correlation between the surface free energy and the particle size distribution of $Al(OH)_3$ powder in sodium aluminate solution system, having agreement with result in Ref. [17]. So, it is reasonable to employ the industrial $Al(OH)_3$ powder as the object for measuring surface free energy of $Al(OH)_3$ with any particle size.

2) Liquid surface tension

The surface tensions of the sodium aluminate solution with different compositions at 298 K and 333 K were measured, as shown in Fig. 2. The liquid surface tension increases linearly with the rise of Na_2O concentration and decreases obviously with the elevation of caustic ratio. This is mainly attributed to the fact that the liquid viscosity increases with the elevation of the solute dissolved in sodium aluminate solution, rendering the increment of contractility vertically acting on the surface of liquid [7]. Meanwhile, the liquid surface tension decreases with the increase of temperature because attractive forces among the molecules weaken as the distance between the molecules increases and the thermal motion of the molecules intensifies with the increase of temperature.

The structure of aluminate anions in solution with different compositions was characterized by infrared spectroscopy, in order to further understand the underlying reasons of the changes in liquid surface tension. Figure 3 shows that the peak shape and intensity of IR spectra of sodium aluminate solution change

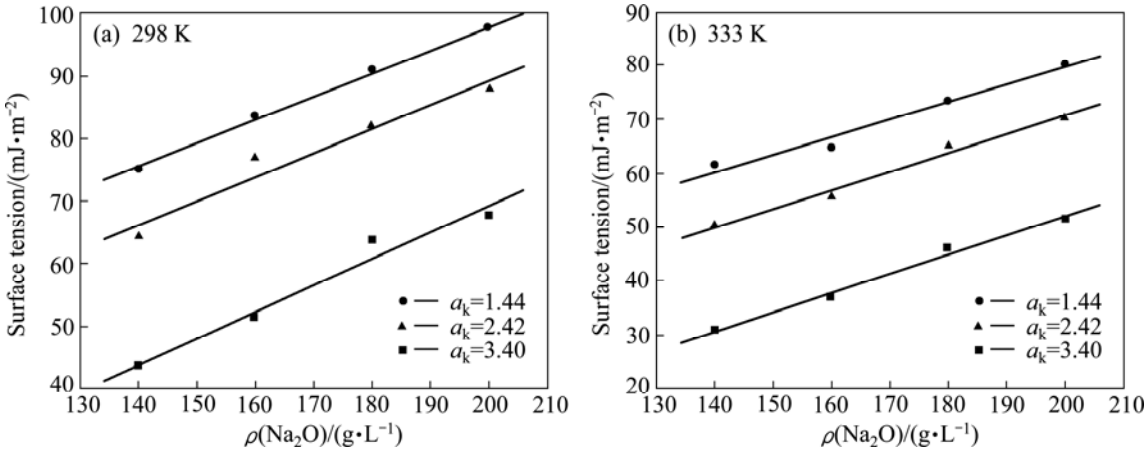

Fig. 2 Effects of solution composition and temperature on surface tension of sodium aluminate solution

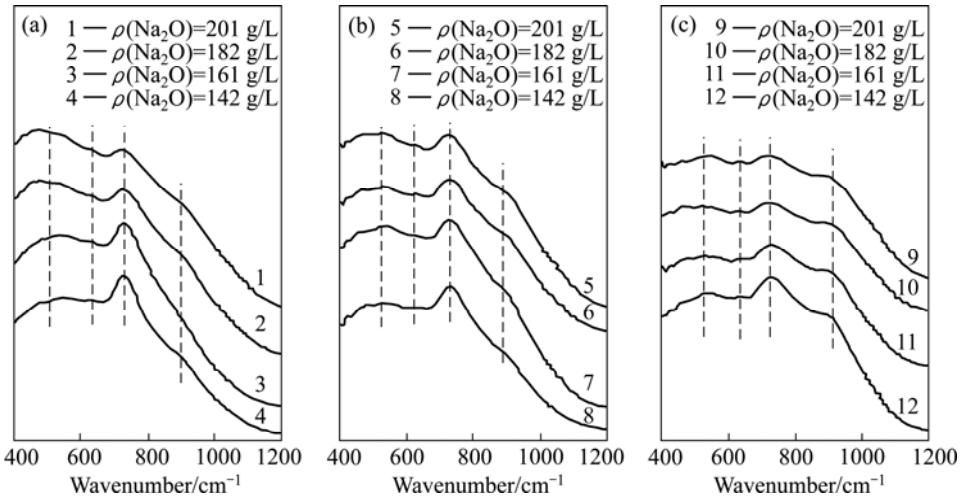

Fig. 3 Infrared spectra of sodium aluminate solution at different concentrations: (a) α_k=3.40; (b) α_k=2.42; (c) α_k=1.44

obviously for different testing samples. For a given caustic ratio of solution, the peak intensity and peak area of the Al−OH vibration of the tetrahedral $Al(OH)_4^-$ at about 720 cm^{-1} [8, 18] reduce and the Al−O−Al vibration of the dimer $Al_2O(OH)_6^{2-}$ at about 550 cm^{-1} [8,18] increases with the rise of Na_2O concentration. The reason is that the tetrahedral aluminate ions dehydrate and polymerize into complex dimer aluminate ions. For a given alkali concentration, the peak intensity and peak area of the Al−O−Al vibration at about 550 cm^{-1} increase and the Al−OH vibration of the polymerized tetrahedral aluminate ions at about 880 cm^{-1} [8,19] decreases with the elevation of caustic ratio. This may be due to the fact that some complex polymerized tetrahedral aluminate ions dehydrate and further polymerize into dimer $Al_2O(OH)_6^{2-}$ when the concentration of OH^- is relatively high. According to the electrochemical properties of sodium aluminate solution [20], the transference number of $Al(OH)_4^-$ is much greater than that of the $Al_2O(OH)_6^{2-}$. Therefore, the polymerization degree of aluminate ions increases with the rise of alkali concentration, resulting in radius increment and thus slow movement of aluminate ions.

3) Solid−liquid interfacial tension

Through trial calculation, it is found that the classic Young' equation was not suitable for calculating the interfacial tension between $Al(OH)_3$ and Bayer liquors. ZHU et al [21] designed a method for characterizing the wetting property of the solid−liquid interface and deduced an expression formula as follows:

$$\gamma_{sl}=\frac{\gamma_{lv}}{2}(\sqrt{1+\sin^2\theta}-\cos\theta),\ 0\leq\theta\leq180^\circ \quad (4)$$

The liquid surface tensions γ_{lv} was obtained as mentioned previously, and according to the above formula, solid−liquid interfacial tensions could be calculated in the case of the values of contact angle between the industrial $Al(OH)_3$ and the synthetic Bayer liquors available. The measured contact angles and the calculated results are listed in Table 2 and Table 3, respectively.

Table 2 Contact angles between industrial $Al(OH)_3$ and Bayer liquors with different compositions

α_k	θ/(°)			
	142 g/L	161 g/L	182 g/L	201 g/L
1.44	31.79	34.23	41.59	46.72
2.42	26.19	29.45	33.17	37.99
3.40	22.88	27.84	28.89	33.84

Table 3 Interfacial tensions γ_{sl} between industrial $Al(OH)_3$ and Bayer liquors under different conditions

T/K	α_k	γ_{sl}/(mJ·m^{-2})			
		142 g/L	161 g/L	182 g/L	201 g/L
298	1.44	10.56	13.42	20.57	26.89
298	2.42	6.29	9.39	12.42	16.99
298	3.40	3.30	5.63	7.49	10.64
333	1.44	8.61	10.38	16.60	22.15
333	2.42	4.94	6.77	9.86	13.55
333	3.40	2.34	4.06	5.41	8.09

It can be seen from Table 3 that the variation trend of solid−liquid interface tension matches that of the liquid surface tension. HERRMANN and STIPETIC [22] reported the interfacial tension of 1250 MJ/m^2, but the method that they used was not presented and the results were not duplicated by subsequent studies. van STRATEN and de BRUYN [23] reported the interfacial tension of (67±20) mJ/m^2 for bayerite and of ~25 mJ/m^2 for pseudo-boehmite, while ROSSITER et al [11] reported the interfacial tension of (45±6) mJ/m^2 for gibbsite at 333 K. It should be noted that the liquor used by HERRMANN and STIPETIC [22] was 10^{-3} mol/L NaOH and that by ROSSITER et al [11] was ~4 mol/L NaOH, and 1.96−3.14 mol/L $Al(OH)_3$. While the liquors used in this work were 4.58−6.48 mol/L NaOH and 3.18−4.5 mol/L $Al(OH)_3$. Therefore, the determined interfacial tensions in this work are reasonable referring to Ref. [24], in which the values of interfacial tensions vary in the range of 0−100 mJ/m^2 for other molecules.

As the precipitation process of Bayer liquors is remarkably influenced by the solubility of $Al(OH)_3$ corresponding to its particle size, it is necessary to study the relationship between $Al(OH)_3$ solubility and particle size in the synthetic Bayer liquors.

3.2 Relationship between $Al(OH)_3$ solubility and particle size in synthetic Bayer liquors

The relationship between solubility and particle size, originally derived for vapor pressures in liquid−vapor systems by THOMSON in 1871, utilized later by GIBBS, and applied to solid−liquid systems by OSTWALD (1900) and FREUNDLICH (1926), may be expressed as follows [25]:

$$\ln\left[\frac{C}{C^*}\right]=\frac{2M\gamma_{sl}}{\upsilon RT\rho r} \tag{5}$$

where C is the solubility of particles of size (radius) r; C^* is the normal equilibrium solubility of the substance; R=8.3 J/(mol·K); T is the thermodynamic temperature; ρ is the density of the solid; M is the molar mass of the solid in solution; γ_{sl} is the interfacial tension of the solid in contact with the solution; υ represents the number of moles of ions formed from one mole of electrolyte. Obviously, for an equilibrium state of solid−liquid system under a specific condition, if the radius of solid particles is less than r, the corresponding solubility is greater than the solubility, and thus the fine particles will be dissolved. That is, r in Eq. (5) can be taken as the critical nucleus size (r_c). For coarse particles, it is feasible that the activity coefficient is not taken into calculation because the actual concentration nearly equals normal equilibrium solubility. However, the differences of activity coefficient cannot be neglected due to the solubility corresponding to fine particles much larger than normal equilibrium solubility. So C and C^* in Eq. (5) should be replaced by their activities:

$$\ln\left[\frac{f\cdot C}{f^*\cdot C^*}\right]=\frac{2M\gamma_{sl}}{\upsilon RT\rho r_c} \tag{6}$$

where f^* and f are the activity coefficients of the sodium aluminate solutions at dissolution equilibrium for coarse $Al(OH)_3$ particle and fine particle with radius r, respectively.

For a given temperature and caustic concentration, f^* and C^* are available from Ref. [26]. The calculation process is as follows: 1) r_c was first designated a value; 2) γ_{sl} and f were then given initial values, respectively; 3) a new value of C was obtained based on Eq. (6); 4) f was calculated according Ref. [26] and γ_{sl} was calculated from Table 3 by the spline interpolation method; 5) repeat steps (3) and (4), when the value difference of C between two adjacent calculations was within 1.0×10^{-4} mole, the last calculated C was output as the result and the calculation ended. Meanwhile, the calculation should meet two conditions: 1) the value of the caustic ratio is not less than 1.0; 2) the designated value of the critical nucleus size is larger than that of the unit cell of 4.66 Å (calculated as spherical particle).

The solubility was plotted as a function of particle size at different temperatures and concentrations of sodium aluminate solution, as shown in Fig. 4. Clearly, the solubility declines sharply for extremely fine particles (<0.1 μm) and then slightly for relatively coarse particles with the increase of particle size, namely, the solubility of fine particles is higher than that of coarse particles. In fact, this is the reason for the property of supersaturation of Bayer liquor. Due to the larger

solubility of fine particles in Bayer liquors, the presence of fine particles is an important factor to limit the depth of precipitation. Furthermore, the solubility of $Al(OH)_3$ particles increases obviously with the rise of Na_2O concentration and temperature, in accordance with that in Ref. [27]. Because the fine particles will be dissolved if the radius is less than r_c, the critical nucleus size r_c increases with the rise of Na_2O concentration and temperature.

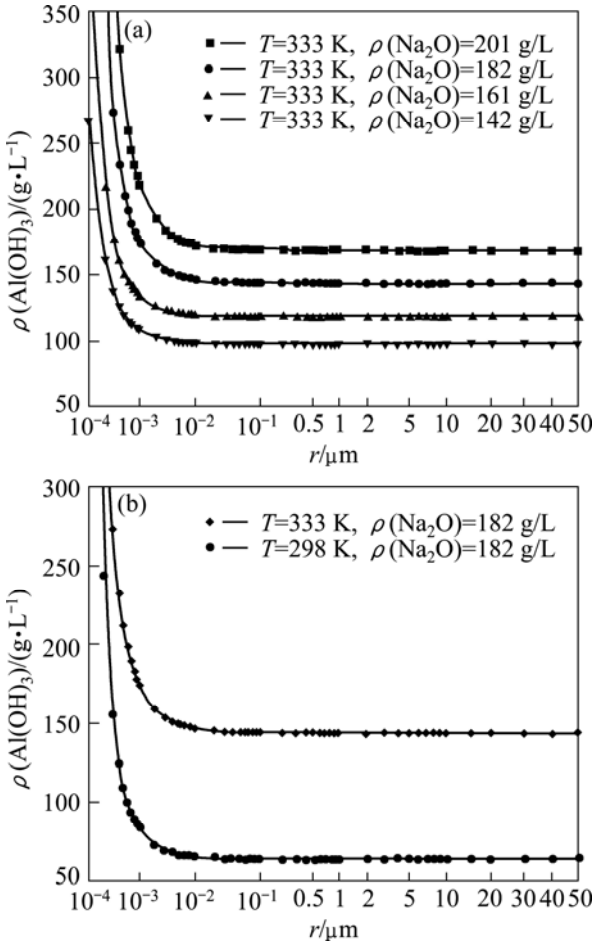

Fig. 4 Relationship between $Al(OH)_3$ solubility and particle size in synthetic Bayer liquors

3.3 Verification of calculation results

As for the critical nucleus size r_c, although there were many studies in literatures, no agreement has been reached. HALFON and KALIAGUINE [28] designated the critical radius of 0.01 μm in their study of kinetics, but it was much larger than the value observed from the micrograph. ZHANG et al [12] and LI et al [13] calculated the critical nucleus size r_c of 1.1−2.0 μm which was also much larger than the observed one. While LOH [29] calculated the critical nucleus size r_c of 0.11 μm using the value of γ_{sl} published by HERRMANN and STIPETIC [22], and ROSSITER et al [11] predicted the critical nucleus size r_c of (0.0012±0.0001) μm at 333 K.

In this work, the values of r_c were calculated to be 0.002 μm and 0.05 μm with Na_2O concentrations of 142 g/L and 182 g/L, respectively, when temperature was 333 K and the caustic ratio was 3.0. It should be noted that the calculation represents the primary nucleation which is different from the secondary nucleation in seeded precipitation. In fact, it is very difficult to measure the critical nucleus size r_c in seeded precipitation process because the actual process involves lots of interrelated physicochemical changes such as nucleation, agglomeration, growth and abrasion. Generally, micrographs of the product were employed to deduce the r_c value by observing the smallest separate particle at near equilibrium state. Therefore, industrial $Al(OH)_3$ seeds were added into the precipitation vessel together with the synthetic Bayer liquor and treated for 70 h under the conditions for our calculation of r_c. The SEM micrographs of the treated product are shown in Fig. 5.

In Fig. 5(a), there are many fine $Al(OH)_3$ particles and part of them attach to coarse $Al(OH)_3$ particles. The value of the smallest isolated particle size on coarse one is measured as 0.002−0.004 μm by scaleplate in image processing, which is close to that calculated. While in Fig. 5(b) fine particles tremendously reduce and the smallest isolated particle size is measured to be about 0.05 μm which almost equals that calculated. Additionally, the primary crystalline in Fig. 5(a) is apparently smaller than that in Fig. 5(b), which means that the particle grows when Na_2O concentration rises, showing the same trend as calculation.

In order to further verify the calculation of r_c, a comparative seeded precipitation experiment was conducted with and without the Ostwald ripening process. The detailed conditions and results are demonstrated in Fig. 6, which illustrates that the Ostwald ripening process can not only enhance the precipitation ratio by 5% but also improve the product particle size distribution. The morphology of obtained $Al(OH)_3$ particles through Ostwald ripening is coarse, uniform and near to spherical, while the product without the Ostwald ripening process is relatively fine and uneven containing a large number of fine particles, indicating that the fine $Al(OH)_3$ particles can be dissolved by Ostwald ripening process. The Ostwald ripening process is caused by the solubility difference between coarse particles and fine particles. In the Ostwald ripening process, the growth of coarse particles relies on the dissolved quality of fine particles, resulting in the uniformity of the product particles. While the thermodynamic driving force increases due to the reduction of total interfacial free energy caused by the increment of particle size, resulting in enhanced precipitation ratio. All mentioned above provide an evidence for our calculation from another aspect.

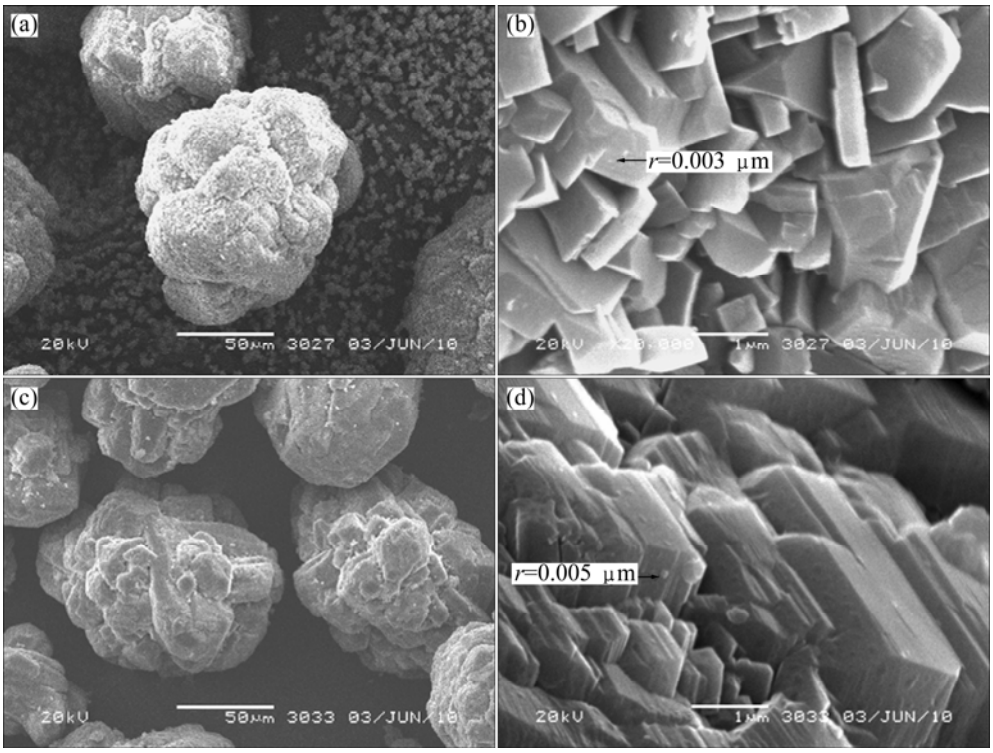

Fig. 5 SEM micrographs of treated product under conditions of 333 K, α_k of 3.0, seed content of 400 g/L, duration of 70 h: (a, b) 142 g/L Na_2O; (c, d)182 g/L Na_2O

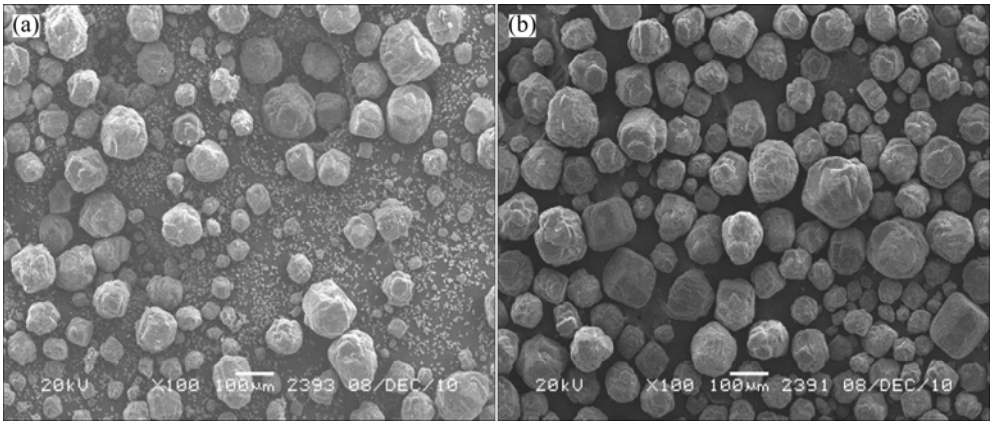

Fig. 6 SEM micrographs of product $Al(OH)_3$ particles by seeded precipitation under conditions of 170 g/L Na_2O, α_{k0} of 1.45, seed content of 600 g/L, initial temperature of 333 K, final temperature of 318 K, duration of 34 h: (a) Maintaining at 318 K for 12 h, η=52%; (b) Ostwald ripening time of 12 h at 333 K, η=57%

4 Conclusions

1) The liquid surface tension of sodium aluminate solution increases linearly with the rise of Na_2O concentration and decreases obviously with the elevation of caustic ratio and temperature. The liquid surface tension closely relates to the structure of aluminate anions.

2) The surface free energy of $Al(OH)_3$ particles is determined to be approximately 48 mJ/m^2 and independent of particle size for macroscopic particles.

3) The relationship between the $Al(OH)_3$ solubility and particle size in the synthetic Bayer liquors are characterized based on Ostwald ripening formula. Reducing particle size and increasing Na_2O concentration and temperature can increase the solubility of $Al(OH)_3$ particles.

References

[1] ANICH I, BAGSHAW T, MARGOLIS N, SKILLINGBERG M. Alumina technology roadmap [C]//Light Metals. Seattle, Washington: TMS Light Metals, 2002: 193−198.

[2] VEESLER S, ROURCE S, BOISTELLE R. About supersaturation and growth rates of hydragillite $Al(OH)_3$ in alumina caustic solutions [J]. Journal of Crystal Growth, 1993, 130(3−4): 411−415.

[3] LI Xiao-bin, WANG Dan-qin, ZHOU Qiu-sheng, LIU Gui-hua, PENG Zhi-hong. Concentration variation of aluminate ions during the seeded precipitation process of gibbsite from sodium aluminate solution [J]. Hydrometallurgy, 2011, 106(1−2): 93−98.
[4] LI H X, ADDAI-MENSAH J, THOMAS J C, GERSON A R. The crystallization mechanism of $Al(OH)_3$ from sodium aluminate solutions [J]. Journal of Crystal Growth, 2005, 279(3−4): 508−520.
[5] BARCZA L, PÁLFALVI-RÓZSAHEGYI M. The aluminate lye as a system of equilibria [J]. Materials Chemistry and Physics, 1989, 21(4): 345−356.
[6] SOAR T J, COUNTER J A, GERSON A R. A static light and X-ray scattering study of supersaturated caustic aluminate liquors [J]. Langmuir, 2000, 16(11): 4784−4791.
[7] WANG Ya-jing, ZHAI Yu-chun, TIAN Yan-wen, HAN Yue-xin, LIU Lian-li. Variation of surface tension of sodium aluminate solution with electrolytic microstructure [J]. The Chinese Journal of Process Engineering, 2003, 3(2): 121−124. (in Chinese)
[8] SIPOS P. The structure of Al(III) in strongly alkaline aluminate solutions—A review [J]. Journal of Molecular Liquids, 2009, 146(1−2): 1−14.
[9] SEYSSIECQ I, VEESLER S, BOISTELLE R, LAMÉRANT J M. Agglomeration of gibbsite $Al(OH)_3$ crystals in Bayer liquors. Influence of the process parameters [J]. Chemical Engineering Science, 1998, 53(12): 2177−2185.
[10] LI Jun, PRESTIDGE C A, ADDAI-MENSAH J. Secondary nucleation of gibbsite crystals from synthetic Bayer liquors: Effects of alkali metal ions [J]. Journal of Crystal Growth, 2000, 219(4): 451−464.
[11] ROSSITER D S, FAWELL P D, ILIEVSKI D, PARKINSON G M. Investigation of the unseeded nucleation of gibbsite, $Al(OH)_3$, from synthetic Bayer liquors [J]. Journal of Crystal Growth, 1998, 191(3): 525−536.
[12] ZHANG Li-chuan, CHEN Qi-yuan, YIN Zhou-lan. Mechanism of homogeneous nucleation in supersaturated sodium aluminate solutions [J]. The Chineses Journal of Nonferrous Metals, 2008, 18(8): 1560−1565. (in Chinese)
[13] LI Jie, CHEN Qi-yuan, YIN Zhou-lan. Studies on the kinetics of unseeded nucleation of aluminum trihydroxide from supersaturated sodium aluminate solutions [J]. Chemical Journal of Chinese Universities, 20003, 24(9): 1652−1656. (in Chinese)
[14] WATTS H L, UTLEY D W. Volumetric analysis of sodium aluminate solutions [J]. Analalytical Chemistry, 1952, 25(6): 864−867.
[15] KWOK D Y, NEUMANN A W. Contact angle measurement and contact angle interpretation [J]. Advances in Colloid and Interface Science, 1999, 81(3): 167−249.
[16] OWENS D K, WENT R C. Estimation of the surface free energy of polymers [J]. Journal of Applied Polymer Science, 1969, 13(8): 1741−1747.
[17] LI Hui-xin, ADDAI-MENSAH J, THOMAS J C, GERSON A R. The influence of Al(III) supersaturation and NaOH concentration on the rate of crystallization of $Al(OH)_3$ precursor particles from sodium aluminate solutions [J]. Journal of Colloid and Interface Science, 2005, 286(2): 511−519.
[18] MOOLENAAR R J, EVANS J C, MCKEEVER L D. The structure of the aluminate ion in solutions at high pH [J]. Journal of Physical Chemistry, 1970, 74(20): 3629−3636.
[19] TARTE P. Infra-red spectra of inorganic aluminates and characteristic vibrational frequencies of AlO_4 tetrahedra and AlO_6 octahedra [J]. Spectrochimica Acta Part A: Molecular and Biomolecular Spectroscopy, 1967, 23(7): 2127−2143.
[20] LI Xiao-bin, WANG Dan-qin, LIANG Shuan, LIU Gui-hua, PENG Zhi-hong, ZHOU Qiu-sheng. Relationship between electric conductivity and ion structure of sodium aluminate solution [J]. Chemical Journal of Chinese Universities, 2010, 31(8): 1651−1655. (in Chinese)
[21] ZHU Ding-yi, DAI Pin-qiang, LUO Xiao-bin, ZHANG Yuan-chao. Novel characterization of wetting properties and the calculation of liquid−solid interface tension (I) [J]. Science Technology and Engineering, 2007, 7(13): 3057−3062. (in Chinese)
[22] HERRMANN E, STIPETIC J. Thermodynamic properties of $Al(OH)_3$ in Bayer liquors [J]. Inorganic Chemistry, 1950, 262: 258−287. (in France)
[23] van STRATEN H A, de BRUYN P L. Precipitation from supersaturated aluminate solutions. II. Role of temperature [J]. Journal of Colloid and Interface Science, 1984, 102(1): 260−277.
[24] SÖHNEL O, GARSIDE J. Precipitation: Basic principles and industrial applications [M]. Sydney: Butterworth-Heinemann, 1992: 35−48.
[25] MULLIN J W. Crystallization, fourth edition [M]. Oxford: Butterworth-Heinemann, 2001: 108−110.
[26] LI Xiao-bin, YAN Li, ZHOU Qiu-sheng, LIU Gui-hua, PENG Zhi-hong. Thermodynamic model for equilibrium solubility of gibbsite in concentrated NaOH solutions [J]. Transactions of Nonferrous Metals Society of China, 2012, 22(2): 447−455.
[27] JANAÍNA A M P, MARCIO S, ENRICO D, JOSÉ C P, JOSÉ L F M, CRISTIANE A H. The kinetics of gibbsite dissolution in NaOH [J]. Hydrometallurgy, 2009, 96(1−2): 6−13.
[28] HALFON A, KALIAGUINE S. Alumina trihydrate crystallization. Part I. Secondary nucleation and growth rate kinetics [J]. The Canadian Journal of Chemical Engineering, 1976, 54(3): 160−167.
[29] LOH P L W. Secondary nucleation of alumina trihydrate in a bath crystallizer [D]. Perth, Australia: Curtin University, 1988: 4−5.

铝酸钠溶液中氢氧化铝的溶解度与颗粒尺寸的关系

李小斌，阎 丽，赵东峰，周秋生，刘桂华，彭志宏，杨帅帅，齐天贵

中南大学 冶金与环境学院，长沙 410083

摘 要：在铝酸钠溶液晶种分解过程中提高分解率与改善产品质量之间存在难以调和的矛盾，因此研究铝酸钠溶液中氢氧化铝的溶解度与颗粒尺寸的关系是很有必要的。采用红外光谱仪、表面张力仪及接触角仪，测定和计算了 $Al(OH)_3$ 颗粒与铝酸钠溶液的固−液界面性质，并结合 Ostwald 熟化公式，对铝酸钠溶液中 $Al(OH)_3$ 溶解度与其颗粒尺寸之间的关系以及临界核尺寸的变化规律进行了分析。结果表明：三水铝石细粒子的溶解度大于粗粒子的溶解度，且其临界核尺寸随着碱浓度、苛性比及温度的升高而增大，细粒子的存在是限制晶种分解程度的重要因素。

关键词：铝酸钠溶液；$Al(OH)_3$；界面性质；溶解度；临界核尺寸

(Edited by Hua YANG)